Journal of Materials Chemistry A

PAPER

View Article Online
View Journal | View Issue

Cite this: J. Mater. Chem. A, 2014, 2, 17545

One-step synthesis of novel mesoporous three-dimensional GeO_2 and its lithium storage properties†

Haiping Jia, Richard Kloepsch, Xin He, Juan Pablo Badillo, Martin Winter* and Tobias Placke*

Received 30th July 2014
Accepted 27th August 2014

DOI: 10.1039/c4ta03933e

www.rsc.org/MaterialsA

Novel mesoporous three-dimensional GeO_2 was successfully synthesized by a facile one-step synthesis method followed by mixing with graphene using a spray drying process. The well-dispersed mesoporous GeO_2 demonstrates a bean-like morphology (b-GeO_2) with a particle size of 400 to 500 nm in length and 200 to 300 nm in diameter, in which mesopores with an average size of 3.6 nm are distributed. The b-GeO_2 without any additional conductive surface layer shows a high reversible capacity for lithium storage of 845 mAh g^{-1} after 100 cycles, with nearly no capacity fading. When graphene was employed to be mixed with GeO_2 *via* a spray drying method, the electrochemical performance is further significantly improved. The b-GeO_2/graphene composite electrode gives a higher de-lithiation capacity of 1021 mAh g^{-1}, and the capacity retention is measured to be as high as 94.3% after 200 charge–discharge cycles for constant current cycling at 0.2 C, as well as an excellent rate performance, even displaying a reversible capacity of 730 mAh g^{-1} at a rate of 5 C.

1. Introduction

Nowadays, rechargeable lithium-ion batteries (LIBs) are the essential part of the most important energy storage devices for portable electronic devices and electric vehicles.[1–3] In order to meet the requirements of high energy density as well as high power performance, a worldwide effort has been made to develop novel high-performance electrode materials to keep pace with the fast increasing market demands. The relatively low theoretical specific capacity (372 mAh g^{-1}) and poor charging rate capability, in particular at low temperatures, are still the main drawbacks of currently commercialized graphite anode materials.[4,5] Various compounds that form intermetallic phases (so-called "alloys") with lithium have been proposed as alternative anode materials, such as silicon (Si),[6–8] tin (Sn)[9,10] and germanium (Ge).[11] Compared to Si, less attention has been paid so far to Ge due to its higher costs. Nevertheless, its good lithium diffusivity (400 times higher than silicon) and high electronic conductivity (*ca.* 104 times higher than silicon) enable it as a promising anode material for the next-generation LIBs. Currently, researchers report on different structures of Ge-based materials, such as nanotubes,[12] nanowires,[13,14] porous structures[15] and Ge-based composite materials.[11,16] So far, only a few studies focus on GeO_2 as an anode material. GeO_2 is of interest for application as a negative electrode material due to its high theoretical reversible capacity (1125 mAh g^{-1} based on 4.25 mol Li per mol Ge), low operation voltage (0.7 V to 0 V *vs.* Li/Li^+) and higher thermal stability compared to Ge.[17–19] The reaction of GeO_2 with Li involves two steps: (1) $GeO_2 + 4Li \rightarrow Ge + 2Li_2O$; (2) $xLi + Ge \rightleftharpoons Li_xGe$ ($x \leq 4.25$). While the first reaction can be considered as to a large part electrochemically irreversible, resulting in a large irreversible charge loss by formation of Li_2O, the lithiation/de-lithiation reaction in step 2 can be regarded as reversible, providing the discharge capacity of GeO_2. The high irreversible capacity during the first lithiation process, which is related to the formation of Li_2O, is also well-known for SnO_2-based anodes and is one of the main reasons hindering so far the application in commercial lithium-ion batteries.[20] Despite the fact that these metal oxides will have no application in lithium-ion batteries, there is still a vast number of publications on new oxide composites, structures and varieties.[17,21–24] The motivation for this work seems to come from the interest in new materials and their synthesis processes rather than from application in electrochemical power sources.

In general, the synthesis of GeO_2 can be achieved by different methods, including hydrolysis reactions from a Ge precursor, chemical vapor deposition (CVD) and sputter processes. Ngo *et al.* synthesized GeO_2 particles by a sol–gel method, which presented a reversible capacity of around 750 mAh g^{-1} at a rate of 0.1 C.[25] Feng *et al.* reported on GeO_2 films as anode materials which were produced *via* a reactive radio frequency sputtering

University of Münster, MEET Battery Research Center, Institute of Physical Chemistry, Corrensstr. 46, 48149 Münster, Germany. E-mail: tobiasplacke@uni-muenster.de; martin.winter@uni-muenster.de; Fax: +49 251 83-36032; +49 251 83-36032; Tel: +49 251 83-36701; +49 251 83-36031

† Electronic supplementary information (ESI) available. See DOI: 10.1039/c4ta03933e

process at different temperatures. The results showed that the GeO_2 thin film with 10 nm thickness possesses the best electrochemical performance, which gives an initial capacity of 930 mAh g^{-1} with 89% capacity retention after 100 cycles.[26] Guo *et al.* reported a GeO_2/graphene composite anode material prepared *via* a one-step *in situ* chemical reduction synthesis method. This material presented a high reversible capacity of 1000 mAh g^{-1} after 50 cycles with a capacity retention of 90%.[17]

Herein, we present a facile one-step preparation method for mesoporous GeO_2 particles with an average particle size of 500 nm and a bean-like morphology. The bean-like GeO_2 (hereafter abbreviated as b-GeO_2) material without any additional conductive surface layer shows a good cycling performance and good rate capability. When graphene was employed to be mixed with GeO_2 *via* a spray drying method, the electrochemical charge–discharge cycling and rate performance are further significantly improved.

2. Experimental

2.1 Preparation of b-GeO_2

$GeCl_4$ (1.0 mL, Alfa Aesar, 99.999%) was dissolved in ethylene glycol (40 mL, Sigma-Aldrich, 99.8%) under stirring for 30 minutes at room temperature. Then, aniline (1.58 mL, Sigma-Aldrich, 99.5%) was added and vigorously stirred for 2 hours. Afterwards, the precipitate was isolated by vacuum filtration, washed with ethanol and vacuum-dried at 100 °C overnight. Commercial GeO_2 particles (average particle size: 1 μm, BET specific surface area: 0.14 m^2 g^{-1}; Sigma-Aldrich) were investigated for comparison.

2.2 Preparation of GeO_2/graphene composite

Graphene oxide (GO) was synthesized from natural flake graphite (325 mesh, Sigma-Aldrich) by a modified Hummers method (see ESI†).[27,28] The GeO_2/graphene composite was prepared *via* a spray drying method. In a typical process, 0.1 g GeO_2 was homogeneously dispersed in a 25 mL aqueous GO suspension (1 mg mL^{-1}), and then the mixture was transferred into the spray drying device (BÜCHI Mini Spray Dryer B-290), followed by annealing at 500 °C for 4 hours in an Ar atmosphere to generate GeO_2/GSs (GeO_2/graphene sheets).

2.3 Structure and morphology characterization

X-ray diffraction (XRD) measurements were carried out using a Bruker D8 Advance X-ray diffractometer (Bruker AXS GmbH) equipped with a copper target X-ray tube (radiation wavelength: $\lambda = 0.154$ nm).

The morphologies of the samples were observed using a scanning electron microscope (Carl Zeiss AURIGA®, Carl Zeiss Microscopy GmbH). Transmission electron microscopy (TEM, JOEL JEM-100CX) was used to investigate the structure of graphene oxide.

The BET specific surface area and BJH pore diameter distribution have been determined by nitrogen adsorption measurements using an ASAP 2020 (Accelerated Surface Area and Porosimetry Analyzer, Micromeritics GmbH). Before the measurement, the samples were degassed at 120 °C until a static pressure of less than 0.01 Torr (0.0133 mbar) was reached.

Thermogravimetric analysis (TGA) was conducted using a TGA Q5000 IR system (TA Instruments). The measurements were carried out in an oxygen atmosphere in the temperature range of 30 °C to 800 °C at a heating rate of 10 °C min^{-1}.

2.4 Electrode preparation, cell assembly and electrochemical investigations

Composite electrodes were prepared using a composition of 80 wt% GeO_2 active material, 10 wt% of conductive carbon black agent C-nergy Super C65 (Imerys Graphite & Carbon) and 10 wt% of sodium carboxymethylcellulose (CMC, Walocel CRT 2000 PA 12) as a binder. Prior to the dispersion of solid compounds, the binder polymer was dissolved in de-ionized water to obtain a 2.0 wt% solution. An appropriate amount of Super C65 was added to the binder solution and the mixture was further homogenized by stirring. Afterwards, a high-energy dispersion step (Ultra-Turrax T25, 1 hour, 5000 rpm) was employed to eliminate agglomerates and homogenize the mixture. The paste was cast on copper foil by a standard lab-scale doctor-blade technique. The gap of the doctor-blade was set at 120 μm wet film thickness, leading to an average mass loading of 1.08 mg cm^{-2}. After casting, the tapes were transferred into an oven and dried in air for 1 hour at 80 °C. Electrodes with a diameter of 12 mm were cut out and a further drying step was performed under an oil-pump vacuum (<0.1 mbar) at 120 °C for 24 hours. Thereafter, the electrodes were stored in an argon filled glove box (UniLab, MBraun) with water and oxygen contents of less than 1 ppm.

Electrochemical experiments were performed using CR2032-type coin cells with Celgard 2400 as the separator and high-purity metallic lithium (Rockwood Lithium) as the counter electrode. The electrolyte was 1 M $LiPF_6$ in a mixture of ethylene carbonate (EC) and diethyl carbonate (DEC) (3 : 7 in weight ratio). The cells were assembled in an argon-filled glove box with oxygen and water contents less than 10 ppm. The electrochemical performance was evaluated on a Maccor 4300 battery test system at 20 °C. The cut-off voltage was 0.01 V for the charge process (lithiation) and 1.5 V for the discharge process (de-lithiation). The specific capacity was calculated on the basis of the total composite weight, and the C-rate was calculated with respect to a theoretical capacity of 1165 mAh g^{-1} (1 C). In the case of the GeO_2/graphene composite electrode, the theoretical capacity is 1103 mAh g^{-1} (where the theoretical capacity of graphene is 540 mAh g^{-1}. [29] Cyclic voltammetry (CV; 0.01–1.5 V) was performed at a scan rate of 0.02 mV s^{-1} using a VMP multichannel constant voltage–constant current system (Biologic® Science Instrument).

3. Results and discussion

As schematically illustrated in Fig. 1, our synthesis approach of GeO_2 is based on the self-assembly of a germanium precursor chelated by $GeCl_4$ and ethylene glycol in the presence of aniline. Aniline, which acts as a base, may promote the growth and

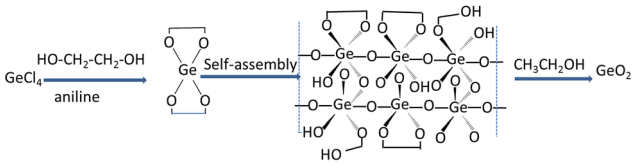

Fig. 1 Schematic illustration of the preparation process of the GeO_2 material.

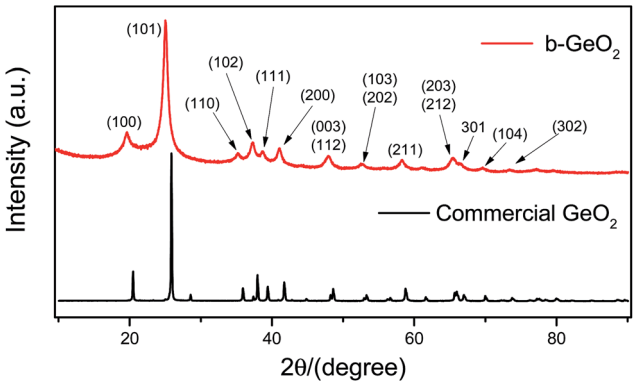

Fig. 2 XRD patterns of the b-GeO_2 product and commercial GeO_2 powders.

stabilization of the chelated germanium precursor by depletion of excess of the acid HCl, which is formed during the chelating process. It should be noted that GeO_2 can readily react with alkali and thus it is important to select a weak base, such as aniline, which can not only absorb the acid arising from the reaction, but also prevent the dissolution of GeO_2. Finally, mesoporous GeO_2 can be spontaneously obtained *via* the removal of the organic phase using ethanol.

The GeO_2 phase of the b-GeO_2 particles was characterized by powder X-ray diffraction analysis, as shown in Fig. 2. The XRD

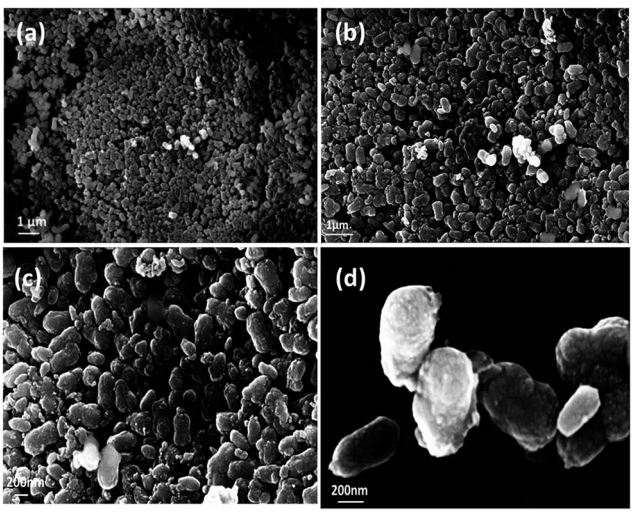

Fig. 3 Low-resolution (a and b) and high-resolution (c and d) SEM images of b-GeO_2.

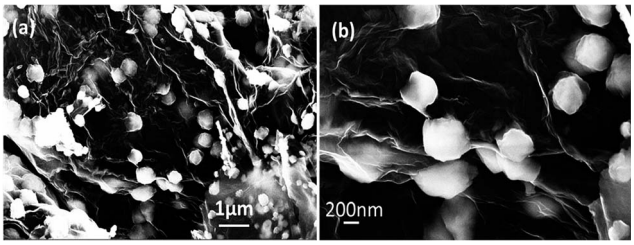

Fig. 4 (a and b) SEM images of the b-GeO_2/graphene composite prepared by the spray drying method.

pattern can be indexed (ICDD# 36-1436) to a hexagonal structure of the *P*3221 (no. 1544) space group, and no impurity phase was observed.[11] Meanwhile the positions of all peaks are in good agreement with commercial GeO_2, except that commercial GeO_2 presents sharper peaks. The synthesis process of our work was completely operated at room temperature without further heat-treatment, which can well explain the existence of broad peaks of the as-prepared material. Furthermore, the broadened peaks are an indication of a very small crystallite size.

The as-prepared GeO_2 shows a bean-like morphology with a particle size of 400 to 500 nm in length and 200 to 300 nm in diameter (Fig. 3a–d). It can be clearly observed that the as-made GeO_2 particles exhibit a uniform morphology. In addition, the well-dispersed GeO_2 shows no tendency to agglomerate, which will be favorable for its electrochemical performance. Furthermore, b-GeO_2 shows a porous structure with a BET specific surface area of 112 $m^2\ g^{-1}$, a pore volume of 0.163 $cm^3\ g^{-1}$ and a pore size of about 3.6 nm, as depicted in Fig. 5, which is typical type H3 of a IV isotherm curve, representing the existence of the porous structure,[30,31] in particular displaying mesopores.

In a further step, we take advantage of graphene (a low-dimensional carbon material with high electronic conductivity and excellent mechanical properties; graphene can contribute to the capacity) to further enhance the electrochemical performance of b-GeO_2.[32,33] A spray drying method was employed to simply mix GeO_2 and graphene (the morphology of graphene oxide is shown in Fig. S1, ESI†). As illustrated in Fig. 4, it can be clearly observed that GeO_2 particles are tightly anchored on or

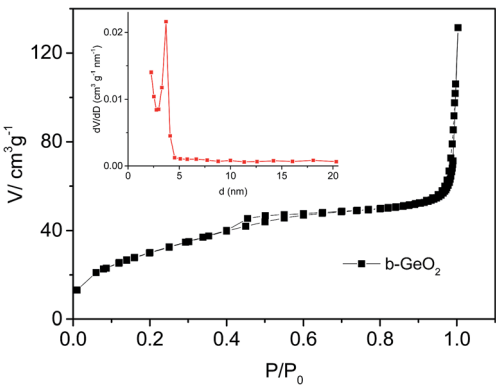

Fig. 5 Nitrogen adsorption/desorption isotherm and pore size distribution of b-GeO_2.

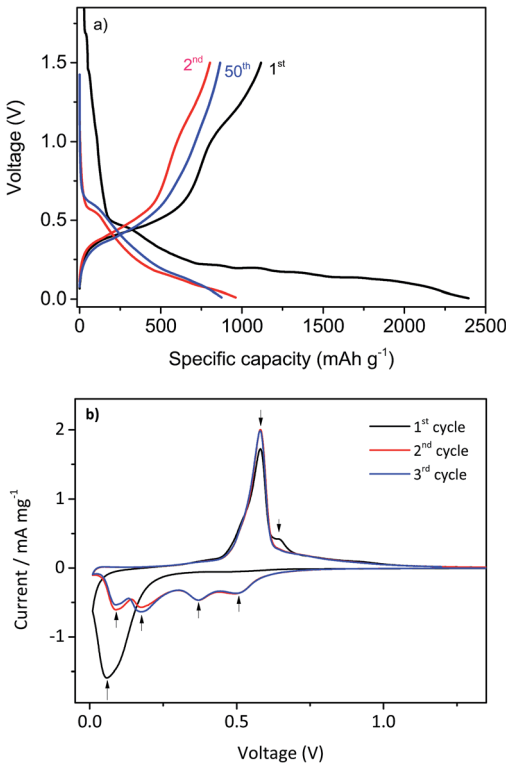

Fig. 6 (a) Representative voltage *vs.* specific capacity profiles of the constant current charge–discharge cycling of b-GeO_2 at 0.1 C (1st cycle) and 0.2 C (2nd cycle and 50th cycle); (b) cyclic voltammetry investigation of the b-GeO_2 electrode at a scan rate of 0.02 mV s^{-1} displaying cycles 1–3. Voltage limits: 0.01 V and 1.5 V.

wrapped within the graphene sheets. Notably, during the mixing process, GeO_2 particles are still homogenously dispersed within or firmly encapsulated by the graphene sheets. To further determine the chemical distribution of the composite, energy dispersive X-ray spectroscopy (EDX) analysis was performed. Fig. S3 (see ESI†) shows the elemental mapping of the corresponding micrograph of the b-GeO_2/graphene composite, in which carbon is settled everywhere, and GeO_2 was found to be homogeneously distributed within the carbon phase.

The amount of graphene was determined by thermogravimetric analysis, as illustrated in Fig. S2 (see ESI†). The weight loss was observed from 200 °C to 700 °C; a rapid mass loss takes place between 500 °C and 650 °C. At 700 °C, the total mass loss is around 12%, so that the mass percentage ratio of graphene and GeO_2 is calculated to be 12% and 88%, respectively.

In Fig. 6a, the voltage *vs.* specific capacity profiles for the charge–discharge cycling process of b-GeO_2 at a rate of 0.1 C in the first cycle (formation cycle) and 0.2 C in the following cycles are presented. With respect to the first cycle, the electrode gives a lithiation capacity of 2394 mAh g^{-1} and a high de-lithiation capacity of 1117 mAh g^{-1}, which is almost equal to the theoretical capacity of GeO_2 (1125 mAh g^{-1}). However, the first cycle efficiency is only about 46.7% (see Table 1), which is quite low compared to currently used graphite-based anode materials. The large capacity loss can be ascribed to the irreversible reaction of GeO_2 during the Li insertion process by formation of Li_2O.[18] Nevertheless, from the second cycle, the efficiency of the electrode was improved significantly and rises nearly to 99% after 50 cycles. The electrochemical lithiation/de-lithiation characteristics of the b-GeO_2 material were determined using cyclic voltammetry (CV), as shown in Fig. 6b. Upon the initial cathodic sweep, a broad reduction peak can be observed at about 0.05 V. It is proposed that the reaction of GeO_2 with Li involves two steps: (1) $GeO_2 + 4Li \rightarrow Ge + 2Li_2O$; (2) $xLi + Ge \rightleftharpoons Li_xGe$ ($x \leq 4.25$). In the case of the first anodic potential sweep, one sharp oxidation peak around 0.55 V and a small broad peak at 0.65 V are revealed, which correspond to the Li extraction reaction. The subsequent cycles show four reduction peaks at 0.50 V, 0.36 V, 0.18 V and 0.09 V, which can be related to the lithium alloying reaction to form different Li_xGe alloys, as described by eqn (1),[34,35] and only one oxidation peak at about 0.55 V, which are in good agreement with the electrochemical characteristics of metallic Ge.

$$\text{Lithiation: } Ge \rightarrow Li_9Ge_4 \rightarrow Li_7Ge_2 \rightarrow Li_{15}Ge_4 \rightarrow Li_{22}Ge_5 \quad (1)$$

In order to demonstrate the improved electrochemical performance of b-GeO_2 and its composite electrodes (b-GeO_2/graphene), commercial GeO_2 powder was studied under the same conditions for comparison. Fig. 7a shows the de-lithiation capacity curves as well as the Coulombic efficiency curves for the charge–discharge cycling of b-GeO_2, b-GeO_2/graphene and commercial GeO_2 at a charge–discharge rate of 0.2 C (the first cycle is conducted at a rate of 0.1 C). Although commercial GeO_2 provides a high initial reversible capacity of 1182 mAh g^{-1}, a rapid capacity fade occurs from the very beginning of cycling, most likely due to the large volume variation, which results in the pulverization and electronic detachment of the active material. In contrast, the b-GeO_2 electrode reveals a significantly improved cycle stability, which demonstrates a high reversible capacity of 845 mAh g^{-1} after 200 cycles, with nearly no capacity fading (according to the capacity of the 2nd cycle, see Table 1). The improved cycling performance can be ascribed to the existence of the mesoporous structure, which can offer sufficient inner space to absorb the volume changes of GeO_2. By mixing GeO_2 with graphene, the initial Coulombic efficiency, cycling performance as well as reversible capacity is further improved. The electrode gives a higher de-lithiation capacity of 1021 mAh g^{-1} with an initial efficiency of 56.4%, and the capacity retention is measured to be as high as 94.3% after 200 cycles. Moreover, from the second cycle, it is observed that the reversible capacity of the b-GeO_2/graphene composite received a remarkable improvement. The coulombic efficiency is above 99.3% from the second cycle. The significantly improved electrochemical performance of the composite is mainly related to its stabilized whole structure, in which the GeO_2 nanoparticles are firmly anchored on or wrapped within the graphene sheets. Together with the good flexibility of the graphene sheets, this composite material might effectively accommodate the big volume changes of GeO_2 during lithiation. In addition, graphene can not only improve the electronic conductivity of GeO_2

Table 1 Representative values for the de-lithiation capacity (1st, 2nd, and 201st cycle), coulombic efficiency (1st, 2nd, and 201st cycle) and capacity retention (201st cycle; related to the 2nd cycle) of commercial GeO_2, b-GeO_2 and b-GeO_2/graphene anode materials. Data correspond to the constant current cycling performance in Fig. 6a

	Cycle	b-GeO_2/graphene	b-GeO_2	Commercial GeO_2
De-lithiation capacity (0.1 C)/mAh g^{-1}	1st	1131	1117	1182
Coulombic efficiency/%		56.4	46.7	53.2
De-lithiation capacity (0.2 C)/mAh g^{-1}	2nd	1074	803	1146
Coulombic efficiency/%		99.3	83.5	96.1
De-lithiation capacity (0.2C)/mAh g^{-1}	201st	1043	845	514
Coulombic efficiency/%		99.8	98.8	99.7
Capacity retention after 200 cycles/%	201st	94.3	96.3	25.5

and therefore raise its utilization efficiency, but also contribute to the specific capacity of the composite.

Fig. 7b shows the rate capability of commercial GeO_2, b-GeO_2 and b-GeO_2/graphene anode materials. The b-GeO_2/graphene electrode delivers higher rate capability than the other electrodes, especially at high specific currents. It shows a high reversible capacity of 730 mAh g^{-1} even at 5 C, while b-GeO_2 and commercial GeO_2 only maintain 300 mAh g^{-1} and 180 mAh g^{-1}, respectively. In particular, the charge–discharge profile of the b-GeO_2/graphene composite exhibits a stable voltage plateau at about 0.2 V for lithium insertion at the high rate of 5 C (as shown in Fig. S4†), which is much higher than the metallic lithium potential. In contrast, the voltage of b-GeO_2 and commercial GeO_2 presents a quick drop towards 0 V during lithium uptake, which may result in the formation of metallic lithium or even lithium dendrites on the surface of the anode and therefore results in safety issues. As mentioned above, the excellent rate capability of the GeO_2/graphene composite benefits from its uniformly dispersed mesoporous structure, in which the GeO_2 particles are homogeneously distributed on or within the conductive graphene sheets, which also shortens the Li^+ diffusion pathways. The open structure is favorable for fast transport of Li^+ and gives rise to high rate performance.

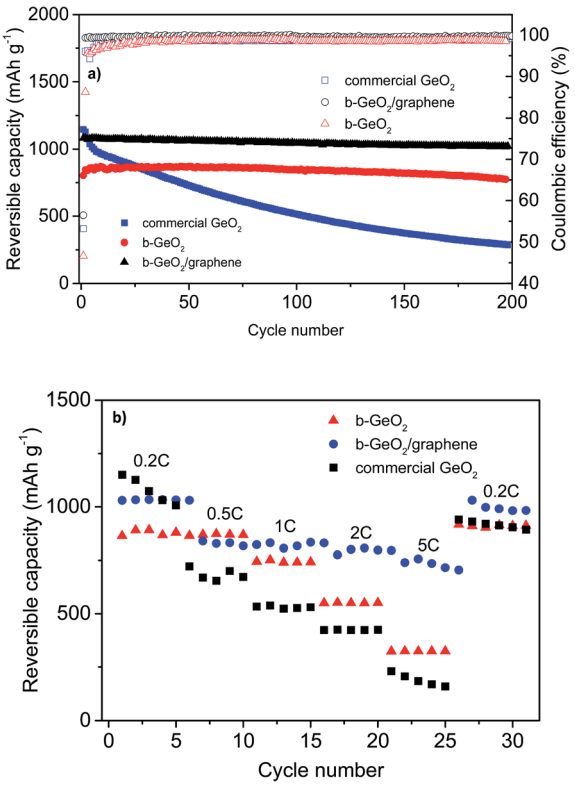

Fig. 7 (a) De-lithiation capacity curves of the constant current cycling of commercial GeO_2, b-GeO_2 and the b-GeO_2/graphene composite at 0.1 C (1st cycle) and 0.2 C (following cycles); (b) the reversible capacity curves of commercial GeO_2, b-GeO_2 and the b-GeO_2/graphene composite at different specific charge–discharge currents (C-rate investigation).

4. Conclusions

In summary, a 3D mesoporous GeO_2 material with a unique morphology was designed and developed *via* a facile and one-step synthesis process. The obtained mesoporous GeO_2 particles present a bean-like morphology (b-GeO_2), and display a good electrochemical charge–discharge cycling performance and rate capability for the lithiation/de-lithiation process. When graphene was employed *via* a spray drying method, the electrochemical performance of the b-GeO_2/graphene composite was further significantly improved. The b-GeO_2/graphene electrode gives a higher de-lithiation capacity of 1021 mAh g^{-1} at 0.2 C and the capacity retention is measured to be as high as 94.3% after 200 cycles. Furthermore, the composite displays an excellent rate performance even up to a charge–discharge rate of 5 C, where a reversible capacity of 730 mAh g^{-1} is obtained. However, the main drawback of GeO_2, similar to the well-known SnO_2-based anode materials, is its high irreversible capacity during the first lithiation due to the irreversible formation of Li_2O. Nevertheless, there is potential to match these anode materials with Li-rich cathode materials for the application in lithium-ion full cells, in which the excessive Li source from the cathode material may compensate the large Li loss of the anode in the first cycle or with sacrificial metallic Li added to the anode mix. The excellent electrochemical cycling performance, a potential application in lithium-ion full cells and in particular the novel and facile synthesis route to a 3D mesoporous material make the GeO_2 composite an interesting anode material for lithium-ion batteries.

Acknowledgements

The authors wish to thank the German Research Foundation for funding this work in the project "WeNDeLIB" (Priority Programme 1473; Materials with New Design for Improved Lithium Ion Batteries). Furthermore, we gratefully acknowledge the supply of materials by Imerys Graphite & Carbon and Rockwood Lithium. We would also like to thank Wei Wei from Max Planck Institute (Polymer Research) for the constant help for TEM measurements.

References

1 J. B. Goodenough and Y. Kim, *J. Power Sources*, 2011, **196**, 6688–6694.
2 J. F. Liang, W. Wei, D. Zhong, Q. L. Yang, L. D. Li and L. Guo, *ACS Appl. Mater. Interfaces*, 2012, **4**, 454–459.
3 R. Wagner, N. Preschitschek, S. Passerini, J. Leker and M. Winter, *J. Appl. Electrochem.*, 2013, **43**, 481–496.
4 M. N. Obrovac and L. Christensen, *Electrochem. Solid-State Lett.*, 2004, **7**, A93–A96.
5 S. Hossain, Y. K. Kim, Y. Saleh and R. Loutfy, *J. Power Sources*, 2003, **114**, 264–276.
6 Y. Yu, L. Gu, C. Zhu, S. Tsukimoto, P. A. van Aken and J. Maier, *Adv. Mater.*, 2010, **22**, 2247–2250.
7 H. P. Jia, P. F. Gao, J. Yang, J. L. Wang, Y. N. Nuli and Z. Yang, *Adv. Energy Mater.*, 2011, **1**, 1036–1039.
8 W.-R. Liu, N.-L. Wu, D.-T. Shieh, H.-C. Wu, M. H. Yang, C. Korepp, J. O. Besenhard and M. Winter, *J. Electrochem. Soc.*, 2007, **154**, A97–A102.
9 W. M. Zhang, J. S. Hu, Y. G. Guo, S. F. Zheng, L. S. Zhong, W. G. Song and L. J. Wan, *Adv. Mater.*, 2008, **20**, 1160–1165.
10 M. Winter, J. O. Besenhard, J. H. Albering, J. Yang and M. Wachtler, *Prog. Batteries Battery Mater.*, 1998, **17**, 208–214.
11 K. H. Seng, M.-H. Park, Z. P. Guo, H. K. Liu and J. Cho, *Angew. Chem., Int. Ed. Engl.*, 2012, **51**, 5657–5661.
12 M.-H. Park, Y. Cho, K. Kim, J. Kim, M. Liu and J. Cho, *Angew. Chem., Int. Ed.*, 2011, **50**, 9647–9650.
13 C. K. Chan, X. F. Zhang and Y. Cui, *Nano Lett.*, 2008, **8**, 307–309.
14 Y.-D. Ko, J.-G. Kang, G.-H. Lee, J.-G. Park, K.-S. Park, Y.-H. Jin and D.-W. Kim, *Nanoscale*, 2011, **3**, 3371–3375.
15 L. C. Yang, Q. S. Gao, L. Li, Y. Tang and Y. P. Wu, *Electrochem. Commun.*, 2010, **12**, 418–421.
16 R. A. DiLeo, S. Frisco, M. J. Ganter, R. E. Rogers, R. P. Raffaelle and B. J. Landi, *J. Phys. Chem. C*, 2011, **115**, 22609–22614.
17 W. Wei and L. Guo, *Part. Part. Syst. Charact.*, 2013, **30**, 658–661.
18 J. S. Pena, I. Sandu, O. Joubert, F. S. Pascual, C. O. Arean and T. Brousse, *Electrochem. Solid-State Lett.*, 2004, **7**, A278–A281.
19 Y. Kim, H. Hwang, K. Lawler, S. W. Martin and J. Cho, *Electrochim. Acta*, 2008, **53**, 5058–5064.
20 J. S. Chen, C. M. Li, W. W. Zhou, Q. Y. Yan, L. A. Archer and X. W. Lou, *Nanoscale*, 2009, **1**, 280–285.
21 Z. P. Guo, G. D. Du, Y. Nuli, M. F. Hassan and H. K. Liu, *J. Mater. Chem.*, 2009, **19**, 3253–3257.
22 F. Xiangpeng, L. Xia, G. Xianwei, M. Ya, H. Yong-Sheng, W. Jiazhao, W. Zhaoxiang, W. Feng, L. Huakun and C. Liquan, *Electrochem. Commun.*, 2010, **12**, 1520–1523.
23 W.-M. Zhang, X.-L. Wu, J.-S. Hu, Y.-G. Guo and L.-J. Wan, *Adv. Funct. Mater.*, 2008, **18**, 3941–3946.
24 W. Wei, S. Yang, H. Zhou, I. Lieberwirth, X. Feng and K. Muellen, *Adv. Mater.*, 2013, **25**, 2909–2914.
25 D. T. Ngo, M. G. Chourashiya, S. W. Kim, C. N. Park and C. J. Park, *224th ECS Meeting – Meeting Abstracts*, 2013, #1054.
26 J. K. Feng, M. O. Lai and L. Lu, *Electrochim. Acta*, 2012, **62**, 103–108.
27 W. S. Hummers and R. E. Offeman, *J. Am. Chem. Soc.*, 1958, **80**, 1339.
28 Y. Liang, D. Wu, X. Feng and K. Muellen, *Adv. Mater.*, 2009, **21**, 1679–1683.
29 Y. EunJoo, J. Kim, E. Hosono, Z. Hao-shen, T. Kudo and I. Honma, *Nano Lett.*, 2008, **8**, 2277–2282.
30 Z. Y. Ryu, J. T. Zheng, M. Z. Wang and B. J. Zhang, *Carbon*, 1999, **37**, 1257–1264.
31 M. Kruk and M. Jaroniec, *Chem. Mater.*, 2001, **13**, 3169–3183.
32 S.-L. Chou, J.-Z. Wang, M. Choucair, H.-K. Liu, J. A. Stride and S.-X. Dou, *Electrochem. Commun.*, 2010, **12**, 303–306.
33 K. Evanoff, A. Magasinski, J. Yang and G. Yushin, *Adv. Energy Mater.*, 2011, **1**, 495–498.
34 G. L. Cui, L. Gu, L. J. Zhi, N. Kaskhedikar, P. A. van Aken, K. Mullen and J. Maier, *Adv. Mater.*, 2008, **20**, 3079–3083.
35 K. Min Gyu and C. Jaephil, *J. Electrochem. Soc.*, 2009, **156**, A277–A282.

